Microfluidics and Nanofluidics (2023) 27:13
https://doi.org/10.1007/s10404-023-02624-9

RESEARCH PAPER

Three-dimensional elastomer bellows microfluidic pump

Robert A. Stavins[1] · **William P. King**[1]

Received: 5 November 2022 / Accepted: 6 January 2023 / Published online: 15 January 2023

Abstract
A key challenge for microfluidics is efficient pumping of fluids, which typically requires equipment that is significantly larger than the pumped fluid volume. This paper presents a miniature elastomer bellows pumps that can be integrated with a microfluidic cartridge. The bellows pump features three-dimensional geometries enabled by additive manufacturing in elastomer materials. To explore a large design space and investigate how pump performance depends upon geometry, we parameterized the design space, fabricated 146 pumps, and performed detailed characterization of pump mechanical properties and fluid-pumping performance. Mechanical property measurements of fluid-filled and unfilled pumps showed linear elastic (LE) stiffnesses from 0.15 to 6.4 MPa and critical stresses from 0.06 to 1.86 MPa. The pumps can deliver between 77 µL and 2.4 mL with a single stroke, and pump efficiency is between 54% and 92%, depending on the design. We explore the size, shape, and number of bellows features and the relationship between mechanical design parameters and pump performance. We find that the pumped volume mostly depends upon the radius and height of the bellows pump. Some pumps buckle under compression which limits the consistency of fluid delivery. The fluid-pumping performance strongly depends upon the bellows design and not on the geometry of the connected microchannels into which fluid is pumped. The research highlights opportunities for miniaturization and integration of microfluidic pumps, as well as opportunities for microfluidic components made from additively manufactured elastomers.

Keywords Microfluidic pumps · Additive manufacturing · Elastomer · Digital design · Mechanical properties

1 Introduction

A central function in many lab-on-chip applications is the pumping of fluid through miniature channels; the pumping allows for fluid analytes and reagents to progress from one step to the next. The pumping pressure is typically provided by an external mechanical pump or by an electric field driven by high voltage electronics. Pump miniaturization has long been a challenge for microfluidic systems, and in general, pumping systems are much larger than the volume of pumped fluid, which often results in the size and weight of a microfluidic diagnostic system is governed not by the microfluidics but instead by the support equipment required. This paper reports a concept for a pressure-driven pump based on a deformable bellows that can be integrated with a microfluidic cartridge.

The two most common approaches for microfluidics pumps are electric field-driven pumps and mechanical pumps. Electric fields are widely used for fluid pumping in microfluidic devices, especially electroosmotic micropumps in which the fluid moves relative to a charged surface by applying an electrical field (Hossan et al. 2018). The flow rate and maximum pressure of the pump can vary based the channel diameter and applied voltage and pump configuration, and typical flow rates range from 500 nL/min to 3 mL/min and typical pressures are between 5 and 200 kPa (Hossan et al. 2018). There are many different types of electroosmosis pumps including open-channel pumps, packed-column pumps, porous membrane pumps, and porous monolith pumps (Hossan et al. 2018; Lazar and Karger 2002). Each configuration differs in the range of flow rates and pumping pressures and there are a variety of applications for these pumps including electronics cooling, chromatography, and flow injection (Borowsky et al. 2008; Brask et al. 2005; Cao et al. 2012; Chen et al. 2005, 2014; Gu et al. 2012; Hossan

✉ William P. King
wpk@illinois.edu

[1] Department of Mechanical Science and Engineering, University of Illinois Urbana-Champaign, Urbana, IL 61801, USA

et al. 2018; Lazar et al. 2006; Nie et al. 2007; Razunguzwa and Timperman 2004; Shin et al. 2011; Takamura et al. 2003; Tripp et al. 2004; Yao et al. 2001, 2003; Zeng et al. 2001, 2002). Other types of electric field-driven pumps include electrothermal pumps, induced charge pumps, and dielectrophoretic pumps (Lei et al. 2009; Paustian et al. 2014; Sigurdson et al. 2005). In contrast to microfluidic pumping based on electric fields, microfluidic pumps based on mechanical pumping are based on an external pressure source such as a syringe or peristaltic pump (Oh et al. 2012). External pressure-driven pumping systems can provide advantages over other kinds of pumps such as electric field-driven pump in terms or more selectable flow rates and pressures through electronics and wide ranges of pumped volumes with flow rates from 5 nL/min to 100 s of mL/min. There are many applications for pressure-driven microfluidics including droplet generation, cell culture, and immunoassay analysis (Byun et al. 2014; Kong et al. 2009; Zeng et al. 2013). Integrated pressure-driven pumps are typically connected to an external pneumatic pressure source to actuate the mechanism in the device (Chou et al. 2001; Grover et al. 2003; Kim et al. 2012; Studer et al. 2003). Both electric field-driven pumps and mechanical pumps require large external equipment, in the form of high voltage electronics or an electric motor. The size of this external equipment mitigates some of the advantages that come with the miniaturization of microfluidics.

A key innovation enabling the miniaturization of microfluidic pumps was the use of elastomeric materials. Elastomer-based microfluidic pumps may be fabricated from elastomeric poly(dimethylsiloxane) (PDMS) devices to create deformable structures that can be actuated with pressure to open or close a microchannel (McDonald and Whitesides 2002; Unger et al. 2000). Elastomeric materials are useful for pumps and valves by providing reversibly deformable components that can move when actuated to provide mechanical force or to open and close a fluid channel, for example in the form of a pressure-actuated diaphragm valve in which a thin deformable membrane is assembled between two stiffer layers which create a continuous channel. The valve can be actuated by changing the pressure to flex the membrane and open the channel for flow (Grover et al. 2003; Zhang et al. 2009). A common method to use deformable valves for pumping is to arrange three valves as a peristaltic pump in which a series of wave-like valve actuations are used to pump small volumes of fluid (Zhang et al. 2009). While there are many publications reporting PDMS microfluidic systems, a common drawback of this approach is the relatively narrow range of geometries that can be fabricated due to limitations of the molding process. For a part to be moldable, it must be possible to remove the part from the mold without breaking the part or the mold. Some 3D features such as overhangs cannot be fabricated using molding.

Recent advances in additive manufacturing (AM) provide new opportunities for the introduction of novel materials and geometries for microfluidics that are not possible with molding. AM of elastomer materials enables designs that are highly deformable without fracture (Herzberger et al. 2019). AM elastomers have been applied to a number of biotechnology applications such as tissue scaffolds, vascular repair, and microfluidic immunoassays (Herzberger et al. 2019; Kuang et al. 2018; Mandrycky et al. 2016; Murphy and Atala 2014; Su et al. 2020; Tian et al. 2017). In the case of tissue scaffolds, the AM elastomers are hydrogels that function as structural support for cells being cultured (Mandrycky et al. 2016; Murphy and Atala 2014). For vascular repair, the AM elastomer can serve as a shape-memory material that conform to a desired 3D shape to reform a broken vascular connection (Kuang et al. 2018). One recent publication studied AM of microfluidic components including valves and pumps with simple 3D geometries that resemble conventionally pneumatically actuated microfluidic valves and pumps (Su et al. 2020). These demonstrations highlight the significant opportunities for microfluidic applications based on AM elastomers, and the potential to exploit the design freedom enabled by AM along with deformable materials.

While there has been significant previous work on microfluidic pumping with molded elastomers, there is a lack of publications that investigate microfluidic pumping using AM elastomers. This paper reports the engineering design and mechanical performance analysis of an AM elastomer bellows pump integrated into a microfluidic system. We explore a large design space with 146 unique pump designs that are produced and tested for mechanical properties and fluid-pumping performance.

2 Device design and measurement

Figure 1 shows the design of the bellows pump. Figure 1a shows the three-dimensional (3D) geometry of the bellows pump. The pump is a hollow cylindrical elastomer device that can be filled with liquid and then compressed to pump liquid into a microfluidic channel. Figure 1b shows the cross-section of the hollow device and integration with a rigid base with embedded microfluidic channels. Figure 1c shows an uncompressed bellows pump and a pump deformed upon compression and Fig. 1d shows a cross-section of a liquid-filled bellows pump in the uncompressed and compressed states. When compressed, liquid flows out of the bellows, through the bottom hole, and into microfluidic channels embedded in the rigid base. The elastomer bellows pump and the rigid base are fabricated using additive manufacturing which enables novel 3D geometries. The 3D shape of sinusoidal sidewalls enables

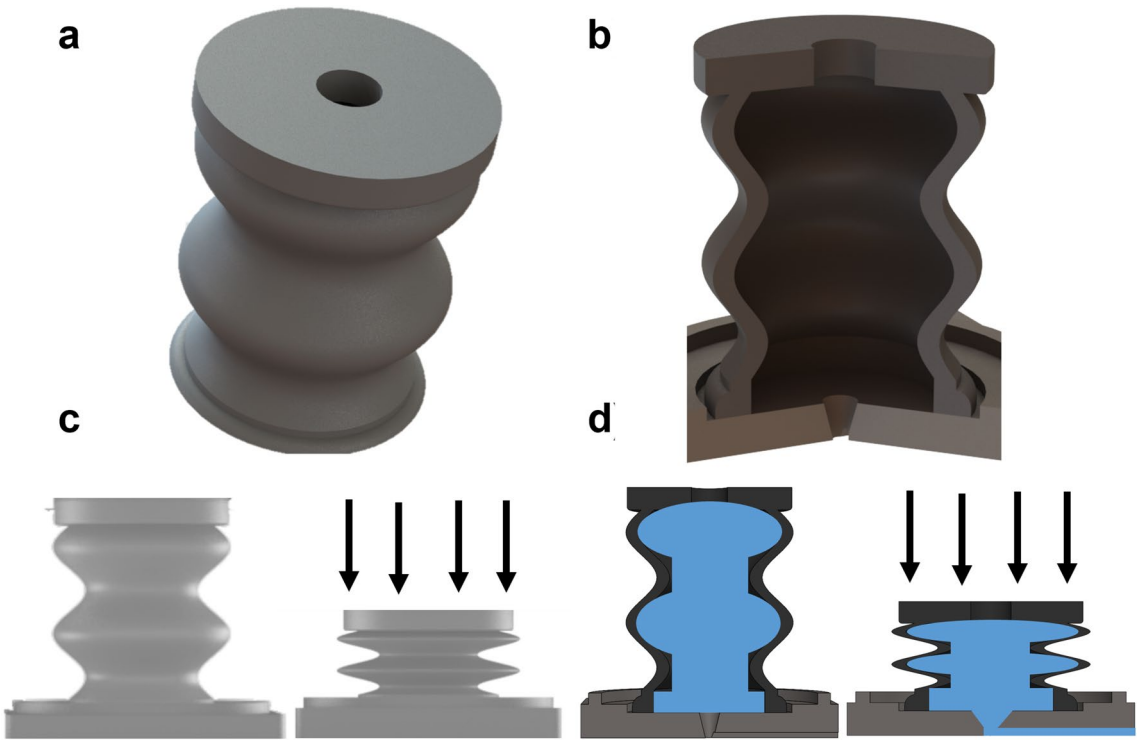

Fig. 1 Bellows pump design and concept of operation. **a** Isometric view of additively manufactured elastomer bellows pump. **b** Cross-section showing the hollow pump and its integration with a rigid base. **c** Side-by-side views of an uncompressed and compressed pump. **d** Cross-section view of liquid-filled pump. Upon compression, liquid flows into microfluidic channels embedded in the rigid base

compression and for the rigid base, the 3D shape of the microchannels enables bellows integration.

Additive manufacturing enables a wide range of bellows geometries. Figure 2 shows the key geometric features and range of parameters explored. The features are the radius of the pump (R), the height of the pump (H), the amplitude of the bellows (α), and the number of bellows (N). We designed 146 unique pumps with design parameters shown in the table of Fig. 2. The design values for the radius were 4.0, 5.0, 6.0, or 7.0 mm; the design values for the amplitude were 0.0, 0.5, 1.0, or 1.5 mm; and the design values for the height were 8.0, 12.0, or 16.0 mm. The shape of the sidewall was parameterized to have either a single concave bellows or convex bellows with 1, 2, or 3 peaks. The case of $\alpha = 0$ mm provides a fifth sidewall design which is a simple cylinder and is equivalent to $N = 0$. All pumps had a sidewall thickness $t = 1.25$ mm. Figures 2(a–e) show examples of different bellows pumps cross-sections with the following parameters: Fig. 2a shows a design with $R = 5$ mm, $\alpha = 1$ mm, $H = 12$ mm, and $N = 2$; Fig. 2b shows a design with $R = 7$ mm, $\alpha = 1$ mm, $H = 12$ mm, $N = 2$; Fig. 2c shows a design with $R = 5$ mm, $\alpha = 1.5$ mm, $H = 12$ mm, $N = 2$; Fig. 2d shows a design with $R = 5$ mm, $\alpha = 1$ mm, $H = 8$ mm, $N = 2$; and Fig. 2e shows a design with $R = 5$ mm, $\alpha = 1$ mm, $H = 12$ mm, $N = 3$. The individual pumps are identified with a label, described in the Supporting Information.

We used an automated, scalable design method to create the part designs in Solidworks. The method starts with a table of design parameters that specifies the design of each part, with four design parameters per pump. Using the Solidworks design table feature, we automatically generated 146 individual computer-aided design (CAD) models the parameter table. We also designed rigid bases to interface with the bellows pumps. The Supplementary Information lists all parts and their design parameters. These bases had a circular housing to fit the bottom of the bellows and integrated microfluidic channels to direct the pumped liquid.

The parts were fabricated on a Carbon M2 printer (Carbon3D). The bellows material was elastic polyurethane (EPU) and the rigid base material was rigid polyurethane (RPU). Both EPU and RPU are two-part resins that undergo an UV cure during the printing process and a post-printing bake to complete the crosslinking (Tumbleston et al. 2015). Around 30 parts could be printed at one time, and the print time was approximately 30 min. After fabrication, we measured the dimensions of 25 parts using calipers to check the outer radius, wall-thicknesses, and heights to ensure the manufacturing was accurate. The measured dimensions of the measured parts were all within 5% of CAD dimensions.

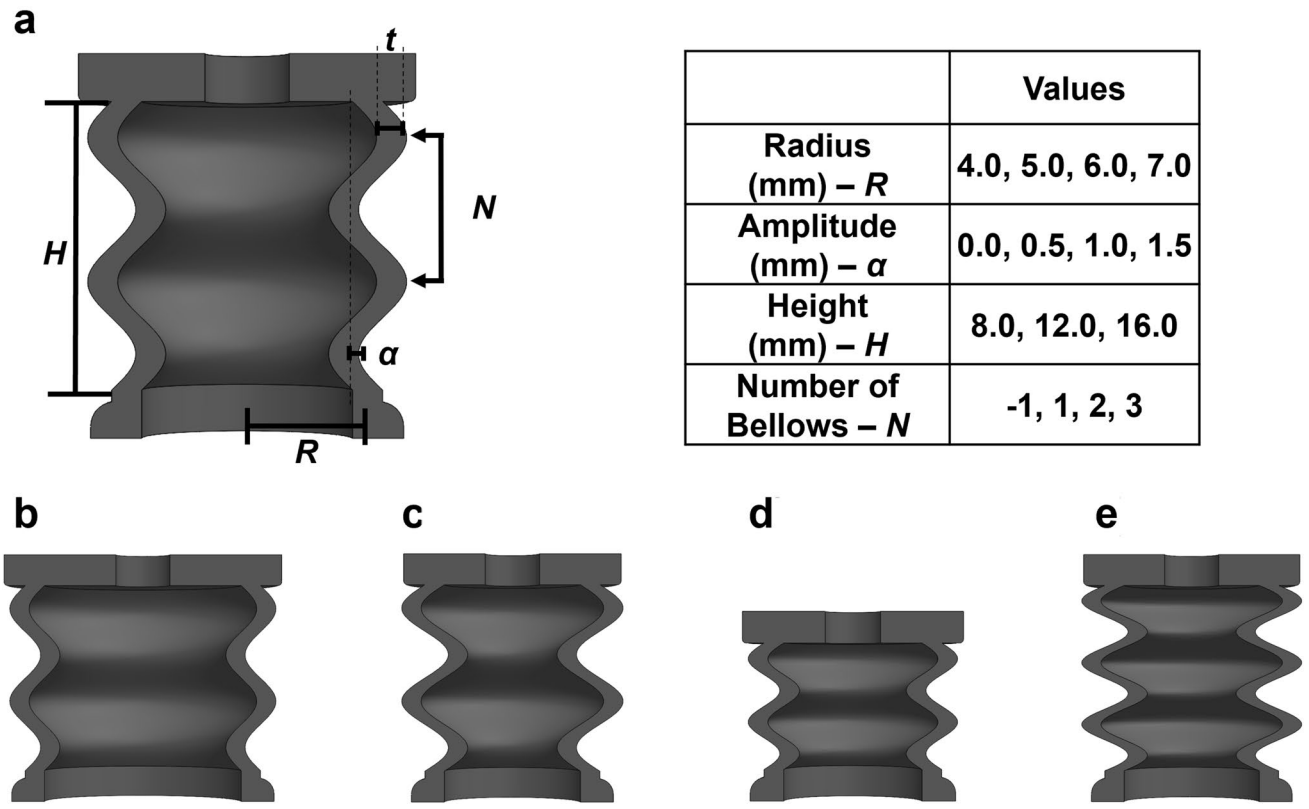

	Values
Radius (mm) – *R*	4.0, 5.0, 6.0, 7.0
Amplitude (mm) – *α*	0.0, 0.5, 1.0, 1.5
Height (mm) – *H*	8.0, 12.0, 16.0
Number of Bellows – *N*	-1, 1, 2, 3

Fig. 2 Bellows pump design parameters and experiment design. **a** Bellows pump cross-section showing design parameters: radius *R*, amplitude *α*, height *H*, number of bellows *N*, and thickness *T*. **b**–**e** Variations of bellows cross-section

The mechanical response of the bellows parts were measured under uniaxial compression to mimic the mechanical behavior during pumping. The measurements were performed in an Instron ElectroPuls E1000 machine with a 2 kN load cell. The parts were first assembled into a rigid base to constrain the bottom of the pump and complete the microfluidic device. The devices were mounted with the flat top of the pump and the bottom of the rigid base in contact with the testing brackets and affixed with double-sided tape to prevent lateral motion during the testing. Each part was tested with a constant 1 mm/s compression rate over a prescribed distance depending on the height of the bellows. For $H = 8$ mm, the compression distance was 5 mm; for $H = 12$ mm the compression distance was 8 mm; for $H = 16$ mm, the compression distance was 11 mm. These strain values approximately correspond to densification onset. After testing, the parts all returned to 100% of their original shape, confirmed with caliper measurements.

Figure 3 shows the rigid base design and Fig. 3a illustrates the fluid flow through the pump under compression. The base is sealed on one size with an adhesive tape, (ARSeal 90,880, Adhesive Research), which completes the microchannel while the pump–base interface is sealed with a UV curable glue (Permabond UV632, Permabond Adhesives) (Berger et al. 2021; Ganguli et al. 2020; Lim et al. 2022). Figure 3b shows how the bellows pump could be integrated into a larger microfluidic system. A compression mechanism can push the fluid from the bellows into connected microfluidic channels for downstream microfluidic analysis. Figure 3c shows the single straight microchannel that receives the pumped liquid in our base design. For some experiments, we varied the microchannel width and depth to measure the impact of fluid resistance on the mechanical properties of the system.

3 Results

Figure 4 shows the mechanical testing results. Figure 4a shows the compression of two different bellows pumps at strain 0 to 0.5 mm/mm. Some of the bellows compressed smoothly with no buckling (top) while some bellows buckled (bottom). Figures 4b and c show measured stress versus strain for four different pumps varying either radius or amplitude. Some tests were performed while the pump was filled with water and some tests were performed for empty pumps. For the family of curves in Fig. 4b, the design parameters are $\alpha = 0$ mm, $H = 16$ mm, $N = 0$ with $R = 4.0$,

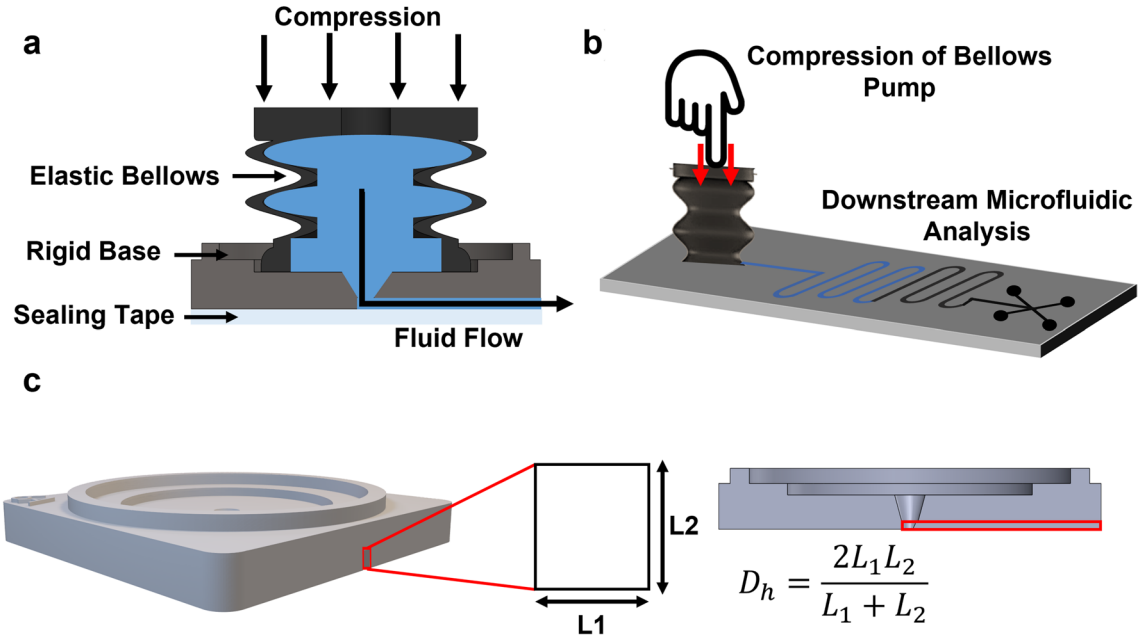

Fig. 3 **a** Schematic of compression test. **b** Schematic of bellows pump integration with a microfluidic system. **c** Bellows base with microchannel, showing the hydraulic diameter

5.0, 6.0, and 7.0 mm. For the family of curves in Fig. 4c, the design parameters are $R = 7$ mm, $H = 16$ mm, $N = 2$ with $\alpha = 0.0$, 0.5, 1.0, and 1.5 mm. Some of the pumps buckled while others did not due to differences in the bellows geometry. The critical stress for buckling increases with radius (Fig. 4b) and decreases with amplitude (Fig. 4c). This result is expected, because for a thin-walled cylinder, the critical stress is proportional to $1/R$ so increasing the radius (Timoshenko et al. 1961).

Figure 5 shows the linear elastic (LE) stiffness and buckling critical stress for all 146 pumps. LE stiffness is defined as the measure of the resistance of the bellows structure to deformation under an applied load. LE stiffness is calculated as the slope of the low strain, linear portion of the stress–strain curve. Figure 5a shows the LE stiffness as a function of bellows radius. Figure 5b shows the LE stiffness plotted as a function of bellows amplitude. Figure 5c shows the critical stress as a function the bellow radius. Figure 5d shows the critical stress as a function of the bellow amplitude. Critical stress is defined by either the stress at which the bellows buckled or the stress at 40% strain were densification of the bellows was observed. Buckling is defined as the stress decreasing to 75% of the maximum value observed within 20% strain. The bellows radius had the largest impacts on the mechanical properties, there is a correlation between increased radius and decreased critical stress and LE stiffness.

The number of bellows affects the pump mechanical properties. Figure 6 shows the numbers of bellows and their effect on critical stress. Figure 6a shows 3D models for bellows pumps with each of the N values with the other three design parameters held constant. Figure 6b shows the experimental data plotted against the bellows radius for each bellows pump that buckled, and the theoretical critical stress plotted as a function of the bellows radius. The theoretical critical stress can be modeled as (Hilburger 2020)

$$\sigma_x = \frac{t}{R}\frac{\gamma E}{\sqrt{3(1-\nu^2)}}, \tag{1}$$

where σ_x is critical stress, t is wall thickness, R is pump radius, the Poisson ratio is $\nu = 0.5$, and the material Young's Modulus, $E = 8.0$ MPa (Carbon3D). The correction factor γ accounts for the pump geometry departure from an ideal cylinder. Our model assigns a unique value γ of for each value of N by using a least squares regression. The measurements agree reasonably well with the model predictions, with better fits that occur for $N = -1, 0, 1$ where there are more data points. Predicting buckling from first principles can be challenging due to the non-linear nature of the buckling process, variability in the geometry of the past as made, and non-ideal mechanical properties (Jiménez et al. 2017; Wagner et al. 2020). Nevertheless, the model generally predicts the magnitude of the critical stress and its geometry dependence. Figure 6c shows the 2D sine wave bellows cross-section for each of the four values of N and given the corresponding value of γ fit in the model. The Supplementary Information

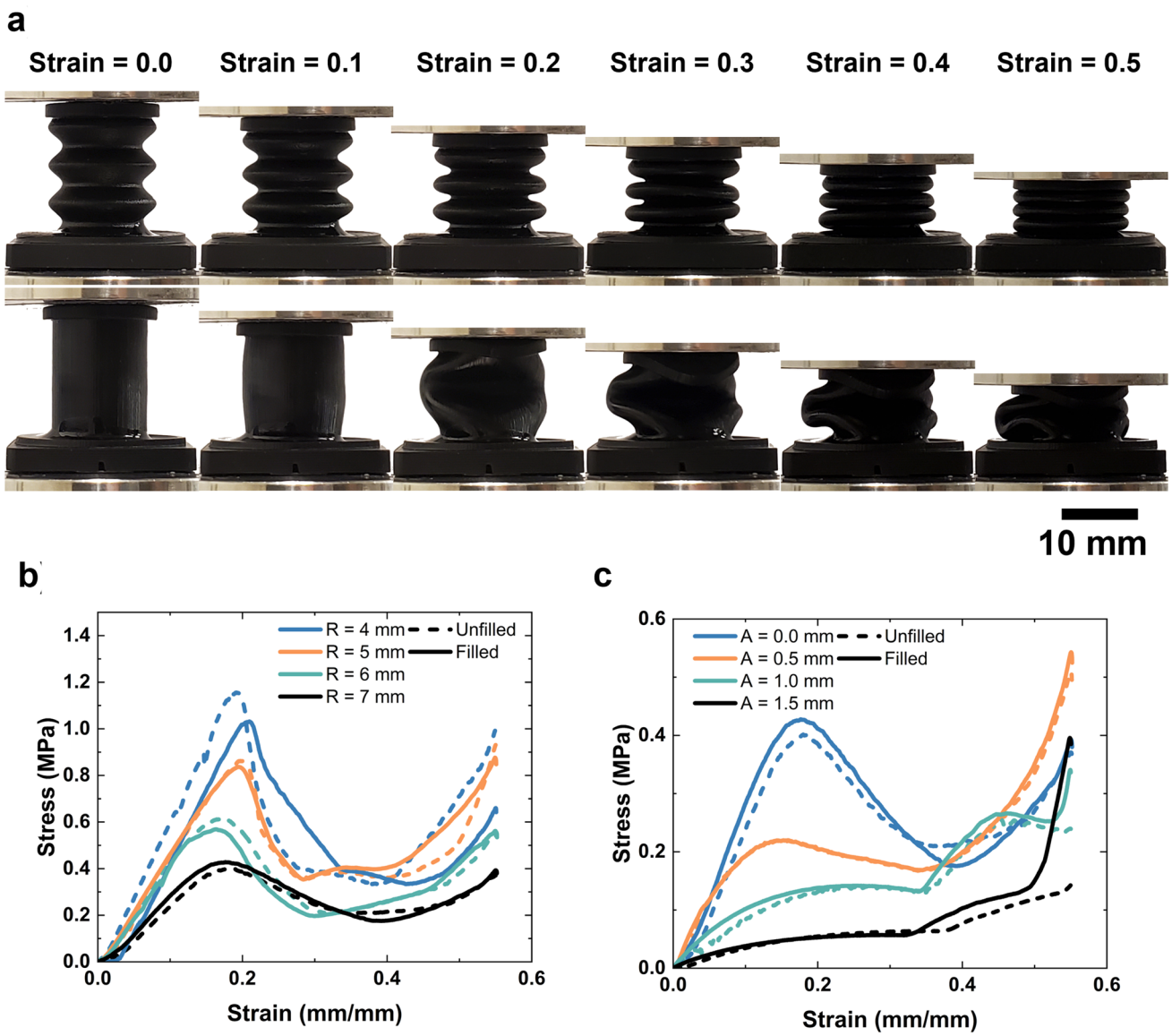

Fig. 4 Compression testing of bellows pumps. **a** Photographs of two bellows during compression testing. **b** Measured stress versus strain for varying radii of water-filled and unfilled pumps. **c** Measured stress versus strain for varying amplitudes of water-filled and unfilled pumps

shows additional analysis of the design parameters and their effect on the pump mechanical properties.

We investigate the mechanical response of the bellows pumps when pumping water into attached microchannels. The pump is actuated by force F_{applied}, the spring force of the bellows that resists deformation is F_{bellows}, and the resistance to fluid flow is $F_{\text{fluid.}}$. Figure 7a shows a force balance schematic for the bellows pump compression, where $F_{\text{applied}} = F_{\text{bellows}} + F_{\text{fluid}}$. We use a conservative estimate of $F_{\text{applied}} = 5$ N which is approximately equal to the smallest maximum force measured for any of the bellows. F_{fluid} is calculated as $F_{\text{fluid}} = R_H * V * A$ where R_h is the hydrodynamic resistance, V is the fluid velocity, and A is the cross-sectional area of the microchannel. Figure 7b shows the ratio $F_{\text{applied}}/F_{fluid}$ as a function of the hydraulic diameter of the microchannel for different channel lengths, L. The fluid resistance F_{fluid} is negligibly small for a large range of operating conditions. The boxed area in the plot shows that for our work the ratio of forces is around 10^5 which means that the pump restoring force is always much larger than the force of the fluid resistance. The channel hydraulic diameter would need to be smaller than about 4 μm for F_{fluid} to approach F_{applied}.

Next, we measured the pump mechanical response when pumping fluid through fluid-filled microchannels of varying hydraulic diameter. Figure 8 shows the stress–strain response of two pumps and five different microchannels with different hydraulic diameters (D_h): 0.150, 0.273, 0.5, 0.667, 0.897 mm. Figure 8a shows the measured stress–strain

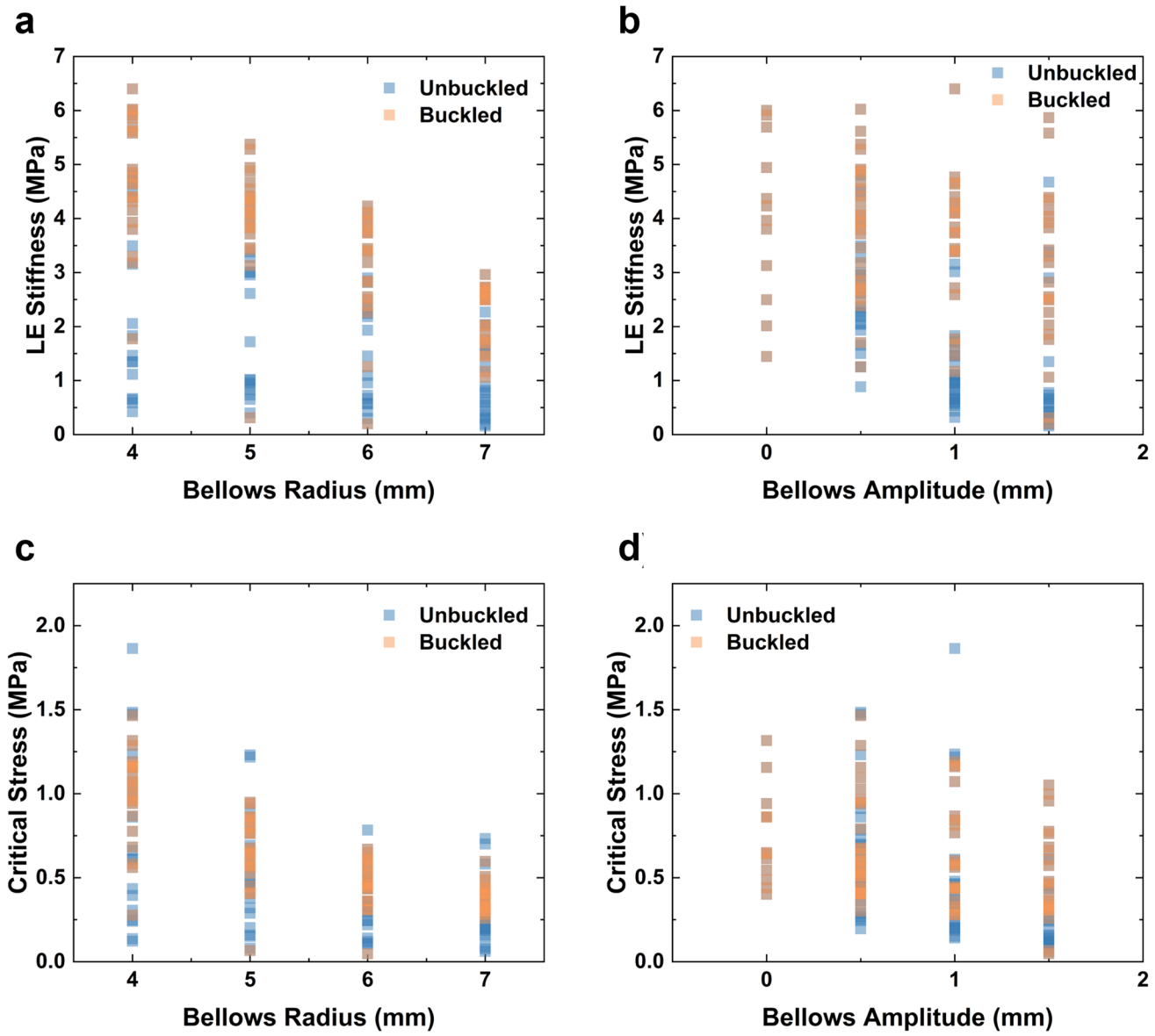

Fig. 5 Summary of compression test results. **a** Linear elastic stiffness as a function of bellows radius. **b** Linear elastic stiffness as a function of bellows amplitude. **c** Critical stress as a function of bellows radius. **d** Critical stress as a function of bellows amplitude. Color indicates whether the bellows buckled or not

response for a pump that buckles, 6L20. At low strain, the mechanical response is nearly identical for all five microchannels. At larger strains, after the pump buckles, there are some differences between the responses, with the smallest D_h parts showing slightly higher stresses than the larger hydraulic diameter parts. The post-buckling differences are likely due to small geometric variations between the pumps which can lead to large differences in buckling and post-buckling behavior. Figure 8b shows the stress–strain response for a pump that did not buckle, 6L23. The pumps have stress values that are very similar for the range of hydraulic diameters considered. Because the mechanical response is insensitive to microchannel hydraulic diameter, we conclude that $F_{\text{applied}} \approx F_{\text{bellows}}$, and the mechanical properties represent only the response of the bellows pumps.

Figure 9 shows an experiment to visualize fluid flow through microchannels during pumping. We designed and fabricated microfluidic devices with long serpentine channels that have volumetric markings, and that can be easily monitored during the stress–strain tests. These devices were assembled with the bellows pumps. Figure 9a shows the experimental procedure, where the liquid-filled pump is compressed at a compression rate of 1 mm/s. The experiments were captured by video and times were recorded for

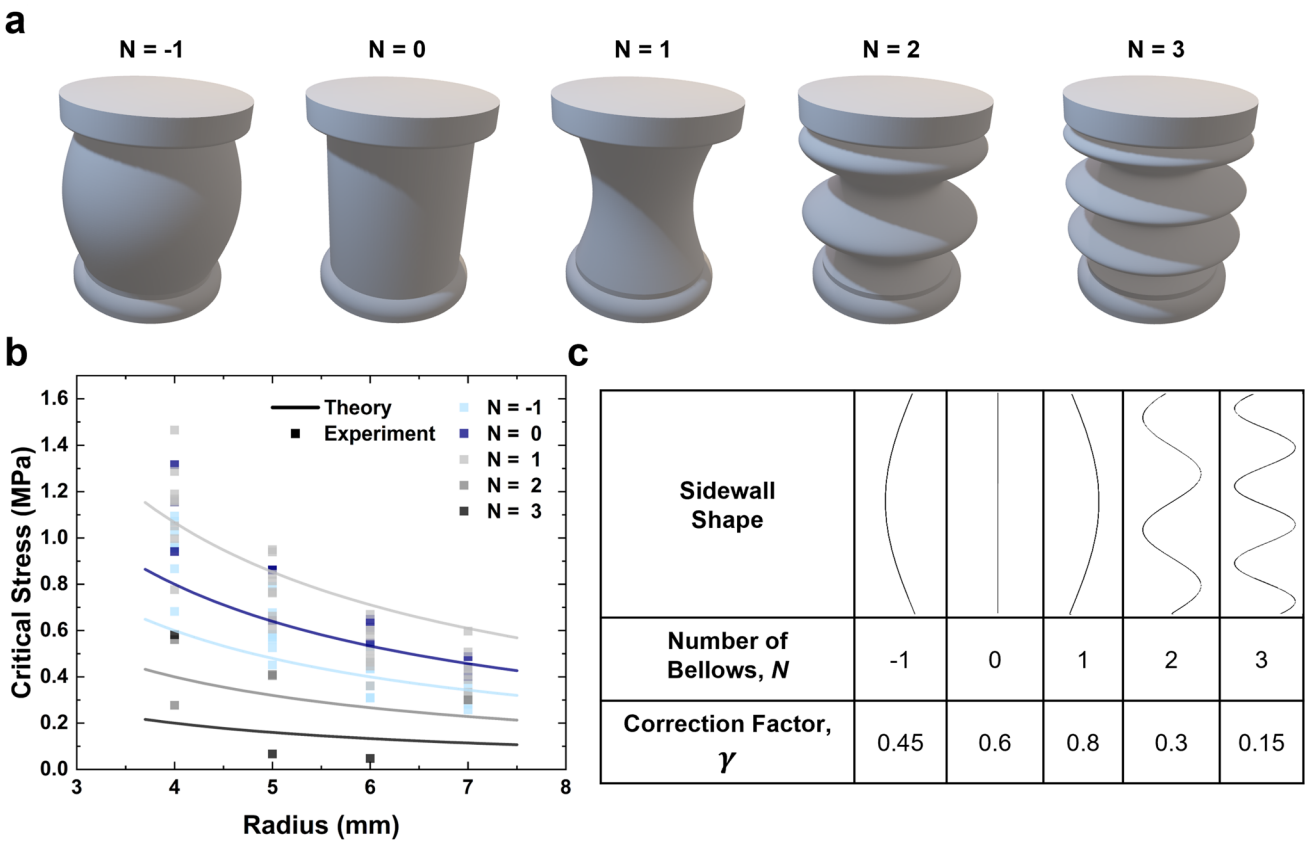

Fig. 6 **a** CAD models of bellows pumps for $N = -1, 0, 1, 2, 3$ with other design parameters held fixed. **b** Measured critical stress for buckled pumps and curve fits. **c** Sidewall shape and correction factor γ corresponding to the given N

each of the volume markings. The pumped volume was associated with the stress and strain at each time. Figure 9b shows the stress versus volume data for five pumps with two of the pumps, 5M11 and 6L20, having higher maximum stresses than the other 3 Pumps (5L32, 6L23, and 7MI3) and have stress maximums located before the maximum pumped volume. The curves shown resemble stress–strain curves as the pumped volume is approximately equal to the strain. The pumps that buckle have a steep increase in stress without high volumes being pumped, but once the buckling occurs there is a region of decreasing stress where most of the volume is pumped. For the pumps that do not buckle, the stress increases with the pumped volume. For consistent pumping, it is desirable to have a smooth curve with relatively low stress such as the 6L23 plot, which makes the pumping more controllable and requires less input power. Figure 9c shows an image of one of the bellows in the test setup, where the arrow marks the location along the serpentine microchannel that the liquid has filled.

The pump efficiency can be defined as the fraction of liquid in the bellows that can be delivered in a single compression. Figure 10 shows an experiment to determine the efficiency of the 146 pump designs. Figure 10a shows the experimental procedure that measures the mass of the empty pump (M1), the mass of the liquid-filled pump (M2), and the mass of the pump after one compression (M3). The mass of the liquid in the pump is the difference between M2 and M1 and the mass released by the pump is the difference between M3 and M2. Figure 10b shows the pumped mass as a function of the held mass M1–M2. The relation between the pumped and held mass is generally linear, with the pumped mass in the range of 60–100% of the held mass. The pumping efficiency is defined as the ratio of pumped volume to held volume, shown in Fig. 10c as a function of pumped volume. For some applications, high efficiency is desired, because this correlates with less wasted liquid. In general, pumps with the highest volumes also have the highest efficiencies. The correlation between pump size and efficiency is likely due to densification of smaller pumps at lower strain.

4 Discussion

We report a novel bellows pump based on a deformable 3D bellows design. We explored a large design space by parameterizing the bellows design and measuring the mechanical

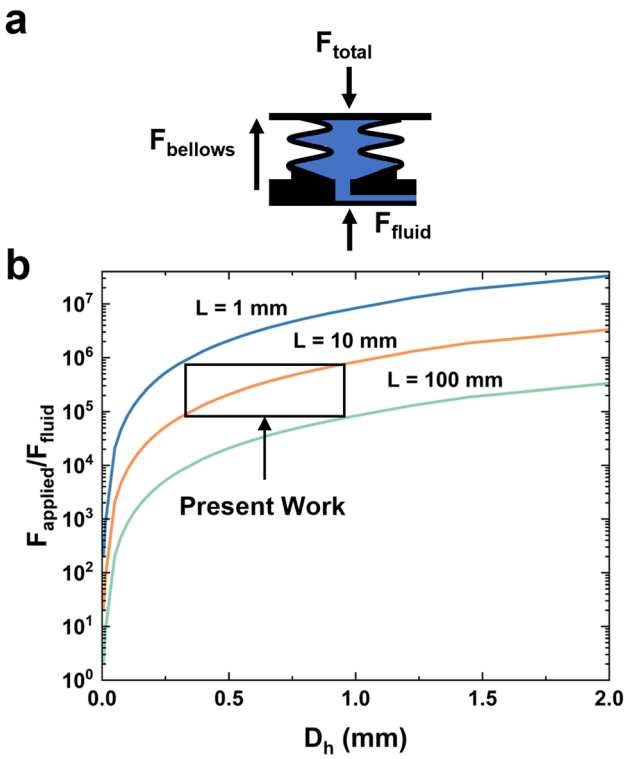

Fig. 7 **a** Schematic showing the force balance on the bellows pump in uniaxial compression. The force applied to the pump is $F_{applied}$, the bellows restoring force is $F_{bellows}$, and the fluid resistance in the channels is F_{fluid}. **b** Plot of the ratio of $F_{applied}$ to F_{fluid} as a function of the hydraulic diameter for three different channel lengths

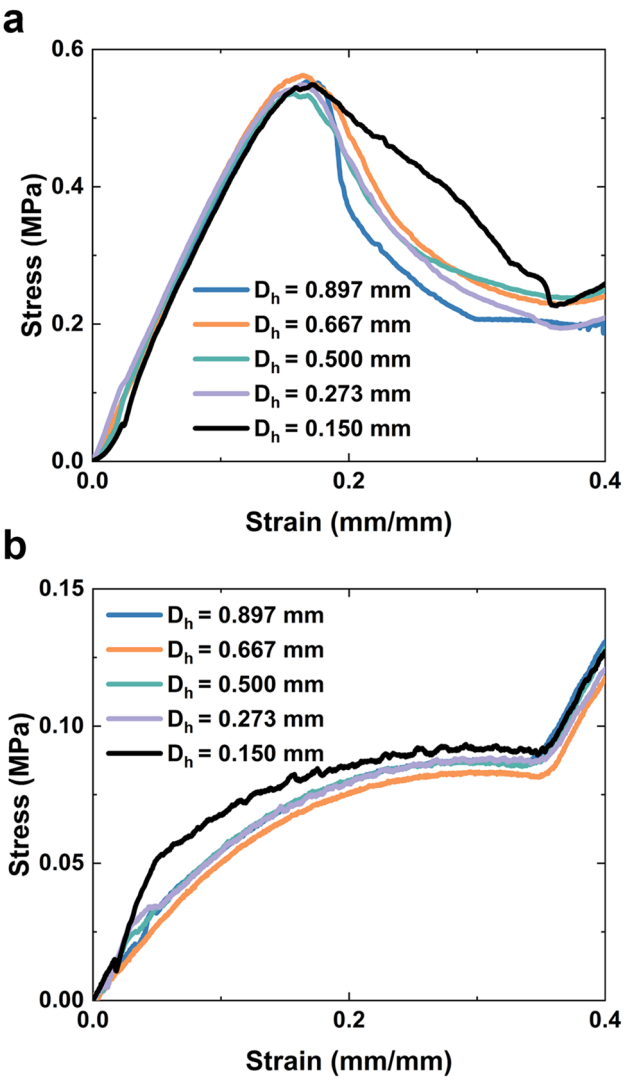

Fig. 8 Stress vs. strain measurements for one pump design and different hydraulic diameters of the microfluidic exit port. **a** A pump design that buckles. **b** A pump design that does not buckle

response of 146 individual pumps and found that the most important design parameters are the pump radius and bellows amplitude. The pumps have LE stiffnesses in the range 0.15–6.4 MPa, and some bellows buckled with critical stress in the range 0.06–1.86 MPa. The parameters that impact on buckling are the number of bellows and the bellows amplitude. In general, softer pumps do not buckle compared to stiffer pumps that buckle more often. It may be desirable to have pumps that do not buckle to provide smooth, linear liquid delivery. The pump volume ranges from 77 µL to 2.4 mL and is mostly determined by radius and height, and is an approximately linear relation between held volume and pumped volume. The range of pumped volume is appropriate for many microfluidic applications such as RNA/DNA analysis, immunoassay tests, sample separation and treatment (Berger et al. 2021; Ganguli et al. 2020; Lim et al. 2022; Ohno et al. 2008). However, some applications require much smaller pumped volumes on the order 10 µL or less such as single-cell sorting or droplet generation (Kobel et al. 2010; Tan et al. 2006), and bellows pump would require significant design modifications to address these applications.

The pump performance compares well with previously reported elastomer pumps. Traditional elastomer pumps involve a series of pneumatic valves cyclically actuated, and typically pump small volumes in the range of a few nL/cycle to 10 s of µL/cycle (Grover et al. 2003; Unger et al. 2000; Zhang et al. 2009). One recent paper showed an elastomer pump driven by an external pneumatic source with a flowrate of 100 nl/cycle (Su et al. 2020). In contrast with previous publications, the bellows pumps of the present study are single actuation pumps rather than continuous flow pumps. For a single actuation pump, the pump performance is characterized by volumetric efficiency rather than flowrate (Borghi et al. 2009; Huang et al. 2020). The bellows pumps have efficiency between 53.6 and 91.8%. It is desirable to maximize the pumping efficiency which minimizes dead volume and wasted liquid. The smallest pumps are the least efficient, which can be attributed to densification that begins a smaller

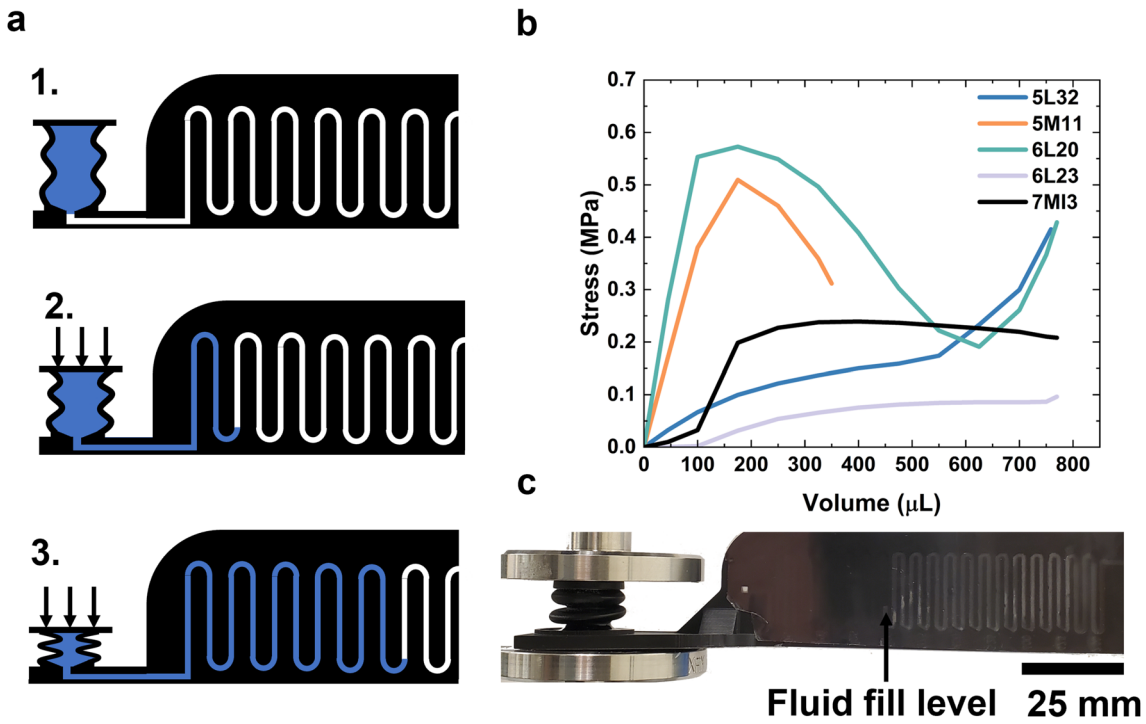

Fig. 9 Liquid pumping during compression. **a** Schematic showing the procedure for pumped volume visualization starting with a full pump that is then compressed to push fluid through a serpentine microchannel. **b** Measured stress versus pumped volume for five different bellows pumps. **c** Photograph of one part during testing

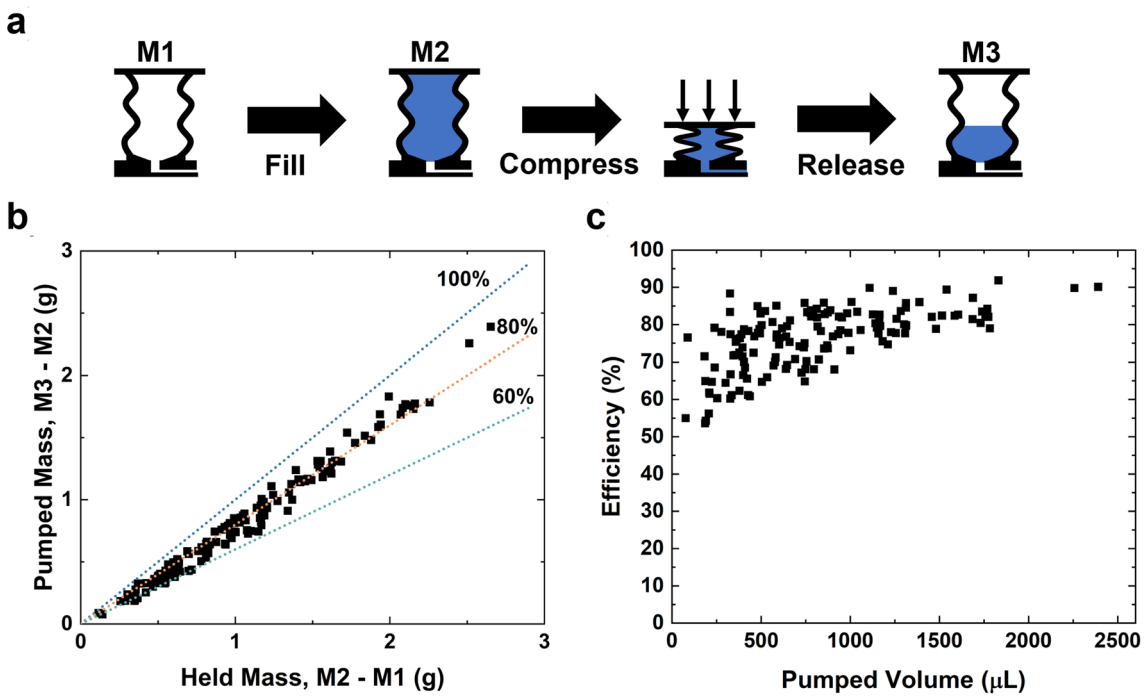

Fig. 10 **a** Schematic for pump efficiency measurement. **b** Measurements of pumped mass versus held mass. **c** Pump efficiency for all 146 designs

strain for small pumps. The densification results from internal contact of neighbor bellows which future research could mitigate with thinner walls or novel 3D designs.

Additive manufacturing offers advantages over molding. The current state of the art for elastomer microfluidics is cast or molded elastomer silicone (McDonald and Whitesides 2002; Raj and Chakraborty 2020) because of its excellent biocompatibility, ease of fabrication, and mechanical property tunability (Kim et al. 2011; Seghir and Arscott 2015). However, the molding process places constraints on the geometries that can be made. In contrast, additive manufacturing enables 3D designs that cannot be molded. Molding requires tooling such that any design changes require new tooling to be fabricated. Because of these limitations, most studies with molded parts consider a small number of device designs (Kobel et al. 2010; Schueller et al. 1999). The toolless nature of AM enables a large design exploration around a given concept, such as the 146 unique designs of the present study. Molding can achieve complex 3D designs only when using multiple processes steps followed by assembly (Iwai et al. 2014, 2011). In contrast, AM enables 3D geometries that cannot be achieved with molding or other traditional manufacturing methods.

The elastomer bellows pump concept is simple and versatile and could be integrated with microfluidic systems in different ways. Figure 11 shows concepts for three different actuation mechanisms for fluid pumping using the bellows. Figure 11a shows actuation using a finger press to apply pressure to pump fluid, Fig. 11b shows actuation by using a screw mechanism, and Fig. 11c shows a simple mechanical lever to actuate the pump. Such manual actuation mechanics could be beneficial for point-of-care diagnostics that require simplicity, small weight and size, and low power operation.

The 3D bellows pump may have advantages over other types of pumps that may require connections to external devices such as mechanical pumps or high voltage supply electronics (Laser and Santiago 2004; Ni et al. 2014; Ren et al. 2016; Wang and Fu 2018; Xu et al. 2020). Our integrated pumps require no external connections for actuation and fit within a small form factor not much larger than a microfluidic cartridge while weighing less than 5 g. A traditional power supply or external pump can weigh 3 kg and take up significantly more space than the microfluidic device itself. For applications such as point-of-care testing, external pumps or electronics with large physical dimensions may be prohibitive. Pumping systems that have been miniaturized for more handheld applications still have a significant physical footprint in the range of 1000 s of cubic centimeters and weights of 100 s of grams (Li et al. 2014; Tang et al. 2018). The 3D bellows pump can reduce the size, weight, and power requirements for a microfluidic system which translates to advantages in portability and cost benefits.

5 Conclusion

We developed a 3D bellows pump from AM elastomer for microfluidics applications. Our design is derived from the traditional bellows shape (Grennell 1838; Welchman 1842). A total of 146 bellows pumps were designed and tested to explore a wide range of parameterized designs. The methods developed here could be extended to other pump designs. Bellows pumps with the four parameters used here could be designed to achieve specific performance requirements, for example constraining the pump performance to be less than a specified applied force.

There are several opportunities for further research. The first opportunity is to explore smaller pumped volumes either with physically smaller pumps or by integrating valves that allow for precise fluid control. We observed that physically smaller pumps have lower efficiencies. To make smaller pumps that maintain relatively high efficiency, it may be possible to reduce the wall thickness of the pumps, which could increase the distance between bellows to delay the densification. We were not able to make bellows pumps with walls thinner than 1 mm, so alternative materials and processes

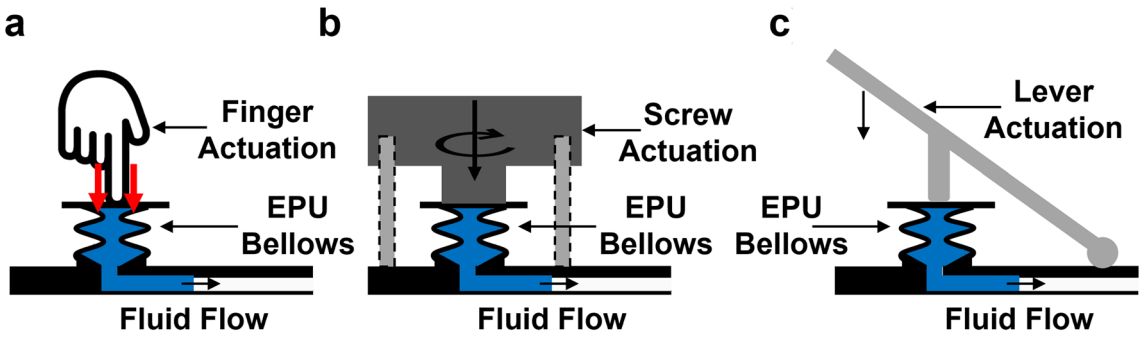

Fig. 11 Concepts for integration of elastomer bellows with different methods of actuation **a** Actuation by applying pressure with a finger **b** Actuation by screwing mechanism **c** Actuation by lever

may need to be. Alternatively, there may be more complex 3D geometries that enable higher performance. For example, topology optimization and origami like folding could create designs that have offset folds that delay densification (Cai et al. 2015; Hunt and Ario 2005; Xing et al. 2022). Finally, further work is required to integrate the pumps with other fluidic components such as valves to make it possible to use multiple bellows pumps in a single system or a single pump with multiple fluids.

Supplementary Information The online version contains supplementary material available at https://doi.org/10.1007/s10404-023-02624-9.

Acknowledgements The authors acknowledge support from the Foxconn Interconnect Technology sponsored Center for Networked Intelligent Components and Environments (C-NICE) at the University of Illinois at Urbana-Champaign.

Author contributions RAS Conducted experiments and analysis. WPK. supervised the research and contributed to analysis. Both authors wrote the manuscript.

Data availability Data is availible upon request.

Declarations

Conflict of interest The authors declare the following financial interests/personal relationships which may be considered as potential competing interests: William P. King is a professor at University of Illinois Urbana-Champaign and the Chief Scientist at Fast Radius where the additive parts were fabricated. This project was conducted in accordance with conflict of management policies at both organizations.

References

Berger J, Aydin MY, Stavins R, Heredia J, Mostafa A, Ganguli A, Valera E, Bashir R, King WP (2021) Portable pathogen diagnostics using microfluidic cartridges made from continuous liquid interface production additive manufacturing. Anal Chem 93(29):10048–10055. https://doi.org/10.1021/acs.analchem.1c00654

Borghi M, Zardin B, Specchia E (2009) External gear pump volumetric efficiency: numerical and experimental. Analysis. https://doi.org/10.4271/2009-01-2844

Borowsky JF, Giordano BC, Lu Q, Terray A, Collins GE (2008) Electroosmotic flow-based pump for liquid chromatography on a planar microchip. Anal Chem 80(21):8287–8292. https://doi.org/10.1021/ac801497r

Brask A, Kutter JRP, Bruus H (2005) Long-term stable electroosmotic pump with ion exchange membranes. Lab Chip 5(7):730. https://doi.org/10.1039/b503626g

Byun CK, Abi-Samra K, Cho Y-K, Takayama S (2014) Pumps for microfluidic cell culture. Electrophoresis 35(2–3):245–257. https://doi.org/10.1002/elps.201300205

Cai J, Deng X, Feng J, Zhou Y (2015) Geometric design and mechanical behavior of a deployable cylinder with Miura origami. Smart Mater Struct 24(12):125031. https://doi.org/10.1088/0964-1726/24/12/125031

Cao Z, Yuan L, Liu YF, Yao S, Yobas L (2012) Microchannel plate electro-osmotic pump. Microfluid Nanofluid 13(2):279–288. https://doi.org/10.1007/s10404-012-0959-x

Chen Z, Wang P, Chang H-C (2005) An electro-osmotic micro-pump based on monolithic silica for micro-flow analyses and electrosprays. Anal Bioanal Chem 382(3):817–824. https://doi.org/10.1007/s00216-005-3130-7

Chen A, Lynch KB, Wang X, Lu JJ, Gu C, Liu S (2014) Incorporating high-pressure electroosmotic pump and a nano-flow gradient generator into a miniaturized liquid chromatographic system for peptide analysis. Anal Chim Acta 844:90–98. https://doi.org/10.1016/j.aca.2014.06.042

Chou H-P, Unger MA, Quake SR (2001) A microfabricated rotary pump. Biomed Microdevices 3(4):323–330. https://doi.org/10.1023/A:1012412916446

Ganguli A, Mostafa A, Berger J, Aydin MY, Sun F, Ramirez SASD, Valera E, Cunningham BT, King WP, Bashir R (2020) Rapid isothermal amplification and portable detection system for SARS-CoV-2. Proc Natl Acad Sci 117(37):22727–22735. https://doi.org/10.1073/pnas.2014739117

Grennell J (1838) Hand Bellows (United States Patent No. 0000872 A). U. S. P. Office

Grover WH, Skelley AM, Liu CN, Lagally ET, Mathies RA (2003) Monolithic membrane valves and diaphragm pumps for practical large-scale integration into glass microfluidic devices. Sens Actuators B 89(3):315–323. https://doi.org/10.1016/S0925-4005(02)00468-9

Gu C, Jia Z, Zhu Z, He C, Wang W, Morgan A, Lu JJ, Liu S (2012) Miniaturized electroosmotic pump capable of generating pressures of more than 1200 bar. Anal Chem 84(21):9609–9614. https://doi.org/10.1021/ac3025703

Herzberger J, Sirrine JM, Williams CB, Long TE (2019) Polymer design for 3D printing elastomers: recent advances in structure, properties, and printing. Prog Polym Sci 97:101144. https://doi.org/10.1016/j.progpolymsci.2019.101144

Hilburger MW (2020) Buckling of thin-walled circular cylinders. NASA Langley Research Center. Report No. NASA/SP-8007-2020/REV 2

Hossan MR, Dutta D, Islam N, Dutta P (2018) Review: electric field driven pumping in microfluidic device. Electrophoresis 39(5–6):702–731. https://doi.org/10.1002/elps.201700375

Huang Y, Ruan J, Chen Y, Ding C, Li S (2020) Research on the volumetric efficiency of 2D piston pumps with a balanced force. Energies 13(18):4796

Hunt GW, Ario I (2005) Twist buckling and the foldable cylinder: an exercise in origami. Int J Non-Linear Mech 40(6):833–843. https://doi.org/10.1016/j.ijnonlinmec.2004.08.011

Iwai K, Sochol RD, Lin L (2011) Finger-powered, pressure-driven microfluidic pump. 2011 IEEE 24th International Conference on Micro Electro Mechanical Systems

Iwai K, Shih KC, Lin X, Brubaker TA, Sochol RD, Lin L (2014) Finger-powered microfluidic systems using multilayer soft lithography and injection molding processes. Lab Chip 14(19):3790. https://doi.org/10.1039/c4lc00500g

Jiménez FL, Marthelot J, Lee A, Hutchinson JW, Reis PM (2017) Technical brief: knockdown factor for the buckling of spherical shells containing large-amplitude geometric defects. J Appl Mech. https://doi.org/10.1115/1.4035665

Kim TK, Kim JK, Jeong OC (2011) Measurement of nonlinear mechanical properties of PDMS elastomer. Microelectr Eng 88(8):1982–1985. https://doi.org/10.1016/j.mee.2010.12.108

Kim J, Kang M, Jensen EC, Mathies RA (2012) Lifting gate polydimethylsiloxane microvalves and pumps for microfluidic control. Anal Chem 84(4):2067–2071. https://doi.org/10.1021/ac202934x

Kobel S, Valero A, Latt J, Renaud P, Lutolf M (2010) Optimization of microfluidic single cell trapping for long-term on-chip culture. Lab Chip 10(7):857–863. https://doi.org/10.1039/B918055A

Kong J, Jiang L, Su X, Qin J, Du Y, Lin B (2009) Integrated microfluidic immunoassay for the rapid determination of clenbuterol. Lab Chip 9(11):1541–1547. https://doi.org/10.1039/B818430E

Kuang X, Chen K, Dunn CK, Wu J, Li VCF, Qi HJ (2018) 3D printing of highly stretchable, shape-memory, and self-healing elastomer toward novel 4D printing. ACS Appl Mater Interfaces 10(8):7381–7388. https://doi.org/10.1021/acsami.7b18265

Laser DJ, Santiago JG (2004) A review of micropumps. J Micromech Microeng 14(6):R35–R64. https://doi.org/10.1088/0960-1317/14/6/r01

Lazar IM, Karger BL (2002) Multiple open-channel electroosmotic pumping system for microfluidic sample handling. Anal Chem 74(24):6259–6268. https://doi.org/10.1021/ac0203950

Lazar IM, Trisiripisal P, Sarvaiya HA (2006) Microfluidic liquid chromatography system for proteomic applications and biomarker screening. Anal Chem 78(15):5513–5524. https://doi.org/10.1021/ac060434y

Lei U, Huang CW, Chen J, Yang CY, Lo YJ, Wo A, Chen CF, Fung TW (2009) A travelling wave dielectrophoretic pump for blood delivery. Lab Chip 9(10):1349–1356. https://doi.org/10.1039/B822809D

Li B, Li L, Guan A, Dong Q, Ruan K, Hu R, Li Z (2014) A smartphone controlled handheld microfluidic liquid handling system. Lab Chip 14(20):4085–4092. https://doi.org/10.1039/C4LC00227J

Lim J, Stavins R, Kindratenko V, Baek J, Wang L, White K, Kumar J, Valera E, King WP, Bashir R (2022) Microfluidic point-of-care device for detection of early strains and B.1.1.7 variant of SARS-CoV-2 virus. Lab Chip 22(7):1297–1309. https://doi.org/10.1039/D2LC00021K

Mandrycky C, Wang Z, Kim K, Kim D-H (2016) 3D bioprinting for engineering complex tissues. Biotechnol Adv 34(4):422–434. https://doi.org/10.1016/j.biotechadv.2015.12.011

McDonald JC, Whitesides GM (2002) Poly(dimethylsiloxane) as a material for fabricating microfluidic devices. Acc Chem Res 35(7):491–499. https://doi.org/10.1021/ar010110q

Murphy SV, Atala A (2014) 3D bioprinting of tissues and organs. Nat Biotechnol 32(8):773–785. https://doi.org/10.1038/nbt.2958

Ni J, Wang B, Chang S, Lin Q (2014) An integrated planar magnetic micropump. Microelectr Eng 117:35–40. https://doi.org/10.1016/j.mee.2013.11.014

Nie F-Q, Macka M, Barron L, Connolly D, Kent N, Paull B (2007) Robust monolithic silica-based on-chip electro-osmotic micropump. Analyst 132(5):417–424. https://doi.org/10.1039/B618386G

Oh KW, Lee K, Ahn B, Furlani EP (2012) Design of pressure-driven microfluidic networks using electric circuit analogy. Lab Chip 12(3):515–545. https://doi.org/10.1039/C2LC20799K

Ohno K-I, Tachikawa K, Manz A (2008) Microfluidics: applications for analytical purposes in chemistry and biochemistry. Electrophoresis 29(22):4443–4453. https://doi.org/10.1002/elps.200800121

Paustian JS, Pascall AJ, Wilson NM, Squires TM (2014) Induced charge electroosmosis micropumps using arrays of Janus micropillars. Lab Chip 14(17):3300–3312. https://doi.org/10.1039/C4LC00141A

Raj MK, Chakraborty S (2020) PDMS microfluidics: a mini review. J Appl Polym Sci 137(27):48958. https://doi.org/10.1002/app.48958

Razunguzwa TT, Timperman AT (2004) Fabrication and characterization of a fritless microfabricated electroosmotic pump with reduced pH dependence. Anal Chem 76(5):1336–1341. https://doi.org/10.1021/ac034956e

Ren YJ, Ma YT, Huang D, Chen J, Feng ZH (2016) Elastic string check valves can efficiently heighten the piezoelectric pump's working frequency. Sens Actuators A 244:126–132. https://doi.org/10.1016/j.sna.2016.04.026

Schueller OJA, Duffy DC, Rogers JA, Brittain ST, Whitesides GM (1999) Reconfigurable diffraction gratings based on elastomeric microfluidic devices. Sens Actuators A 78(2):149–159. https://doi.org/10.1016/S0924-4247(98)00242-8

Seghir R, Arscott S (2015) Extended PDMS stiffness range for flexible systems. Sens Actuators A 230:33–39. https://doi.org/10.1016/j.sna.2015.04.011

Shin W, Lee JM, Nagarale RK, Shin SJ, Heller A (2011) A miniature, nongassing electroosmotic pump operating at 0.5 V. J Am Chem Soc 133(8):2374–2377. https://doi.org/10.1021/ja110214f

Sigurdson M, Wang D, Meinhart CD (2005) Electrothermal stirring for heterogeneous immunoassays. Lab Chip 5(12):1366–1373. https://doi.org/10.1039/B508224B

Studer V, Hang G, Pandolfi A, Ortiz M, French Anderson W, Quake SR (2003) Scaling properties of a low-actuation pressure microfluidic valve. J Appl Phys 95(1):393–398. https://doi.org/10.1063/1.1629781

Su R, Wen J, Su Q, Wiederoder MS, Koester SJ, Uzarski JR, McAlpine MC (2020) 3D printed self-supporting elastomeric structures for multifunctional microfluidics. Sci Adv. https://doi.org/10.1126/sciadv.abc9846

Takamura Y, Onoda H, Inokuchi H, Adachi S, Oki A, Horiike Y (2003) Low-voltage electroosmosis pump for stand-alone microfluidics devices. Electrophoresis 24(1–2):185–192. https://doi.org/10.1002/elps.200390012

Tan Y-C, Cristini V, Lee AP (2006) Monodispersed microfluidic droplet generation by shear focusing microfluidic device. Sens Actuators B 114(1):350–356. https://doi.org/10.1016/j.snb.2005.06.008

Tang S-Y, Zhang X, Sun S, Yuan D, Zhao Q, Yan S, Deng L, Yun G, Zhang J, Zhang S, Li W (2018) Versatile microfluidic platforms enabled by novel magnetorheological elastomer microactuators. Adv Funct Mater 28(8):1705484. https://doi.org/10.1002/adfm.201705484

Tian K, Bae J, Bakarich SE, Yang C, Gately RD, Spinks GM, in het Panhuis M, Suo Z, Vlassak JJ (2017) 3D printing of transparent and conductive heterogeneous hydrogel-elastomer systems. Adv Mater 29(10):1604827. https://doi.org/10.1002/adma.201604827

Timoshenko S, Gere JG, Gere JM (1961) Theory of elastic stability. McGraw-Hill

Tripp JA, Svec F, Fréchet JMJ, Zeng S, Mikkelsen JC, Santiago JG (2004) High-pressure electroosmotic pumps based on porous polymer monoliths. Sens Actuators B 99(1):66–73. https://doi.org/10.1016/j.snb.2003.10.031

Tumbleston JR, Shirvanyants D, Ermoshkin N, Janusziewicz R, Johnson AR, Kelly D, Chen K, Pinschmidt R, Rolland JP, Ermoshkin A, Samulski ET, DeSimone JM (2015) Continuous liquid interface production of 3D objects. Science 347(6228):1349–1352. https://doi.org/10.1126/science.aaa2397

Unger MA, Chou H-P, Thorsen T, Scherer A, Quake SR (2000) Monolithic microfabricated valves and pumps by multilayer soft lithography. Science 288(5463):113–116. https://doi.org/10.1126/science.288.5463.113

Wagner HNR, Hühne C, Janssen M (2020) Buckling of cylindrical shells under axial compression with loading imperfections: an experimental and numerical campaign on low knockdown factors. Thin-Walled Struct 151:106764. https://doi.org/10.1016/j.tws.2020.106764

Wang Y-N, Fu L-M (2018) Micropumps and biomedical applications—a review. Microelectr Eng 195:121–138. https://doi.org/10.1016/j.mee.2018.04.008

Welchman E (1842) Apparatus for Resuscitation (United States Patent No. 0002547 A). U. S. P. Office

Xing J, Luo Y, Deng Y, Wu S, Gai Y (2022) Topology optimization design of deformable flexible thermoelectric devices for voltage enhancement. Eng Optim. https://doi.org/10.1080/0305215X.2022.2108416

Xu L, Wang A, Li X, Oh KW (2020) Passive micropumping in microfluidics for point-of-care testing. Biomicrofluidics 14(3):031503. https://doi.org/10.1063/5.0002169

Yao S, Huber D, Mikkelsen JC, Santiago JG (2001) A large flowrate electroosmotic pump with micron pores. ASME 2001 International Mechanical Engineering Congress and Exposition. https://doi.org/10.1115/IMECE2001/MEMS-23890

Yao S, Hertzog DE, Zeng S, Mikkelsen JC, Santiago JG (2003) Porous glass electroosmotic pumps: design and experiments. J Colloid Interface Sci 268(1):143–153. https://doi.org/10.1016/S0021-9797(03)00730-6

Zeng S, Chen C-H, Mikkelsen JC, Santiago JG (2001) Fabrication and characterization of electroosmotic micropumps. Sens Actuators B 79(2):107–114. https://doi.org/10.1016/S0925-4005(01)00855-3

Zeng S, Chen C-H, Santiago JG, Chen J-R, Zare RN, Tripp JA, Svec F, Fréchet JMJ (2002) Electroosmotic flow pumps with polymer frits. Sens Actuators B 82(2):209–212. https://doi.org/10.1016/S0925-4005(01)01007-3

Zeng Y, Shin M, Wang T (2013) Programmable active droplet generation enabled by integrated pneumatic micropumps. Lab Chip 13(2):267–273. https://doi.org/10.1039/C2LC40906B

Zhang W, Lin S, Wang C, Hu J, Li C, Zhuang Z, Zhou Y, Mathies RA, Yang CJ (2009) PMMA/PDMS valves and pumps for disposable microfluidics. Lab Chip 9(21):3088–3094. https://doi.org/10.1039/B907254C